Journal Pre-proof

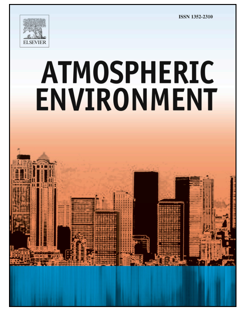

Effect of Flare destruction and removal efficiencies on regional ozone pollution from oil, gas and chemical process industries in Southeast of Texas through CAMx modeling and simulation

Sijie Ge, Sujing Wang, Qiang Xu, Thomas Ho

PII: S1352-2310(20)30067-4

DOI: https://doi.org/10.1016/j.atmosenv.2020.117326

Reference: AEA 117326

To appear in: *Atmospheric Environment*

Received Date: 18 January 2020

Revised Date: 26 January 2020

Accepted Date: 1 February 2020

Please cite this article as: Ge, S., Wang, S., Xu, Q., Ho, T., Effect of Flare destruction and removal efficiencies on regional ozone pollution from oil, gas and chemical process industries in Southeast of Texas through CAMx modeling and simulation, *Atmospheric Environment* (2020), doi: https://doi.org/10.1016/j.atmosenv.2020.117326.

Sijie Ge: Conceptualization, Methodology, Software, Data curation, Writing-Original draft preparation.

Sujing Wang: Visualization, Investigation.

Qiang Xu: Conceptualization, Methodology, Supervision, Writing-Review and Editing, Funding acquisition

Thomas Ho: Supervision, Writing-Reviewing and Editing, Funding acquisition

Graphical Abstract

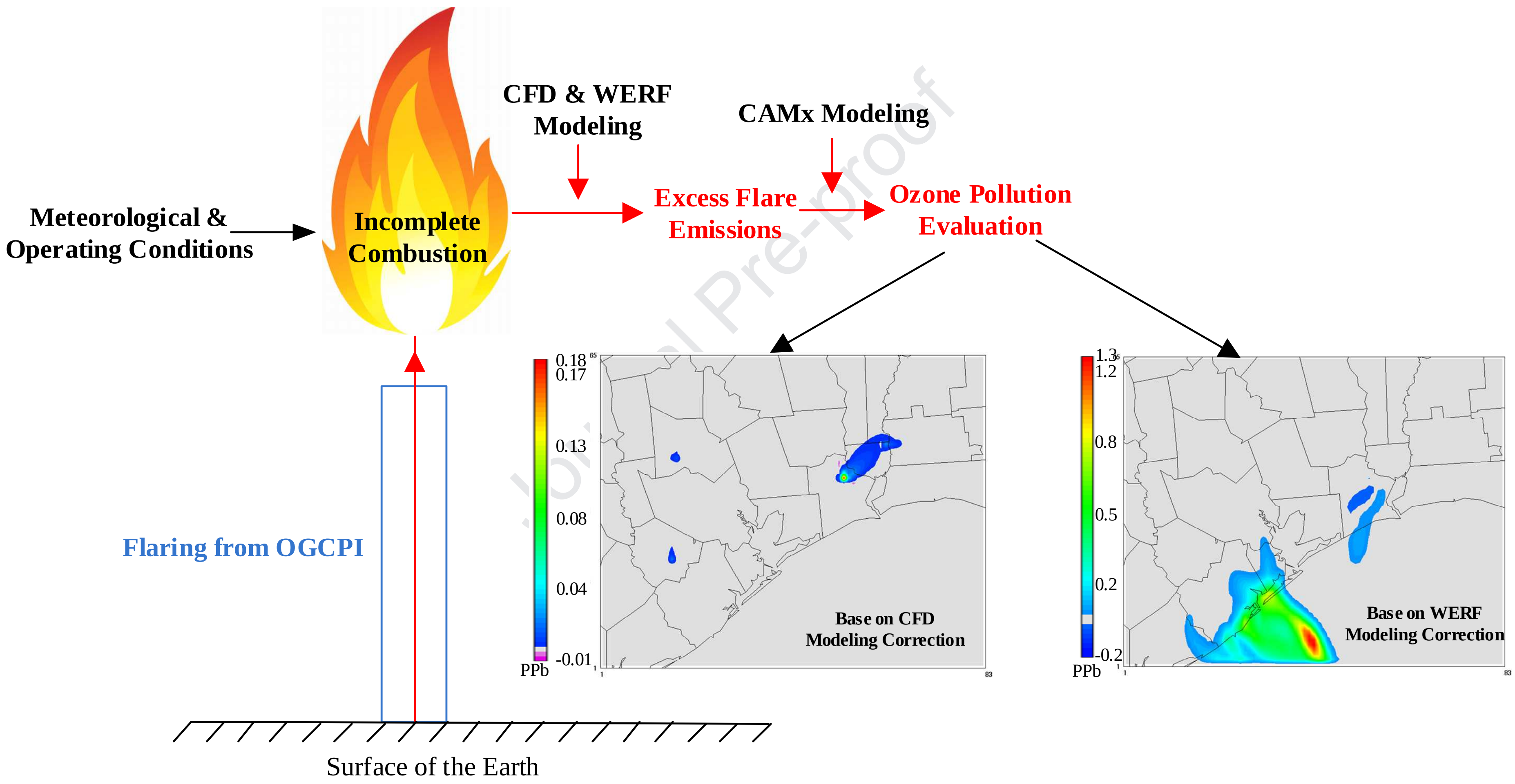

Effect of Flare Destruction and Removal Efficiencies on Regional Ozone Pollution from Oil, Gas and Chemical Process Industries in Southeast of Texas through CAMx Modeling and Simulation†

Sijie Ge[1,2], Sujing Wang[3], Qiang Xu[1,*], Thomas Ho[1]

[1]Dan F. Smith Department of Chemical Engineering, Lamar University, Beaumont, Texas 77710, USA
[2]School of Environment Science and Spatial Informatics, China University of Mining and Technology, Xuzhou, Jiangsu, 221116, China
[3]Department of Computer Science, Lamar University, Beaumont, Texas 77710, USA

Abstract

Flare is the last safety measure for daily operations in oil, gas & chemical process industries (OGCPI). However, an excessive flaring releases large quantity of emissions of VOCs and NO_x, which may suddenly enhance local ozone as a secondary pollution. Normally, the flare destruction and removal efficiency (DRE) of 98 % or 99 % is regulated as the national standard and presumed for industrial practices in the U.S. Unfortunately, real DRE values could be much lower than the standard due to impact factors including various meteorological and operating conditions such as the cross-wind speed, flare jet velocity and heating value of combustion. Thus, it is critically important to explore the sensitivity of the regional ozone impact due to low DREs of OGCPI flare combustions. In this paper, a systematic methodology has been developed to examine ozone impacts due to the low flare DREs, which have never been systematically studied before. The DRE formulas were derived from computational fluid dynamic (CFD) modeling and Water Environment Research Foundation (WERF) results and then employed to recompile the point source emission inventory. After that, comprehensive air quality model with extensions (CAMx) was employede to simulate and quantify local ozone changes impacted by flare emissions of OGCPI. Case studies indicate that the maximum hourly ozone increments due to the low DRE through CFD and WERF modeling is 0.18 ppb and 1.3 ppb, respectively. This study could enrich fundamental understandings of industrial point source emissions and provide the quantitative and valuable support for the ozone pollution caused by OGCPI flare emissions under low DRE instead of standard values.

Keywords: Ozone Pollution; Industrial Emissions; Flare; DRE; CAMx

---

† For publication in *Atmospheric Environment*.

* All correspondence should be addressed to Prof. Qiang Xu (Phone: 409-880-7818; Fax: 409-880-2197; E-mail: Qiang.xu@lamar.edu).

1. Introduction

Industrial flaring is to safely combust off-spec, unusable, or unwanted process streams, which might otherwise be harmful to local environment if directly vented without destructions. The oil, gas and chemical process industries (OGCPI) in the U.S. daily processes millions of cubic feet of hydrocarbon gases (Baukal and Schwartz, 2001; Aalsalem et al., 2018). Thus, a slight decrease in flaring performance will release millions of cubic feet of gaseous emissions into the atmospheric environment. Note that although flaring is a safety measure for plant safety in OGCPI, excessive flaring will generate large amounts of emissions such as NO_x (nitrogen oxides), CO_2, CO, VOCs (volatile organic compounds) especially for high reactive VOCs (i.e., HRVOCs such as ethylene, propylene, acetylene). For instance, an olefin plant with a capacity of 1.2 billion pounds of ethylene productivity per year can easily flare about 5.0 million pounds of ethylene during one single start-up operation (Xu and Li, 2008). Given the 98 % flaring efficiency (TCEQ, 2015), the resultant air emissions include at least 15.4 million pounds of CO_2, 40.0 Klbs CO, 7.4 Klbs NO_x, 15.1 Klbs hydrocarbons, and 100.0 Klbs HRVOC (Xu et.al, 2009). These emissions may cause seriously regional and transient air pollution events as well as negative societal impacts (Ge et al., 2016; Ge et al., 2017; Ge et al., 2018a; Ge et al., 2019). It should also be noted that under adverse meteorological and operation conditions (e.g., strong cross-wind, high jet velocity, or low combustion heating value), the flare destruction and removal efficiency (DRE) can be reduced, and thus the portion of unburned species will be significantly increased (Castiñeira and Edgar, 2008; Singh et al., 2012; Devesh et al., 2014). Among the resultant consequences, one of particular concerns is the increment of unburned VOCs, which transiently elevate local ground-ozone concentrations as a secondary pollution, because ozone is usually generated by photochemical reactions between NO_x and VOCs under sunlight (Cleveland, 1974).

Ground-level ozone poses detrimental effects on human beings and many other living species. For instance, ozone can irritate respiratory system, which includes asthma aggravation, lung function reduction, and permanent lung damage (Kampa, 2008). Thus, ozone is regulated as one of six common pollutants regulated by the Federal Clean Air Act. The U.S. EPA (Environmental Protection Agency of the United States) has set the National Ambient Air Quality Standards (NAAQs) for the ground-level ozone since July 1997. From Oct 1st, 2015, a more stringent ozone standard on the 8-hr average of 70 ppb has been issued (EPA, 2016). Currently, OGCPI flaring practices (American Petroleum Institute, 2008) needs to satisfy the 98 % standard value for DRE. According to EPA regulations, a 98 % DRE or higher could be obtained if the flare operations can be in accordance with 40 CFR Section 60.18 (McDaniel, 1983). Flaring activities (61%) are among the top three HRVOCs emission sources in Texas, USA and thus has much potential to form ozone pollution (Singh et al., 2014). A rapid increase in ozone concentration has been commonly observed at air quality monitoring stations in Houston, Texas, USA. This phenomenon was regarded as a transient high ozone event, which may due to industrial flare emissions (Allen, 2017; Ge et al., 2018b).

In real practices, however, flaring DREs could be lower than the standard value due to impact factors such as the cross-wind speed, jet velocity, heating value of combustion zone (HVCZ) and flare design (Pohl, 1984 and 1985). Recently, Ge et al., 2016 has studied the ozone impacts due to low DREs of multiple olefin plant start-ups via virtual case studies, where the 8-hr ozone increment under the assumed DREs of 95 %, 96 %, 97 % and 98 % have been investigated, respectively. Generally, plant start-up operations should generate the larger amount of flare emissions than that of normal operations; but they have a much less frequency than daily normal operation. Thus, it is still interesting to explore the air quality impact from lower DREs under adverse meteorological and operating conditions during OGCPI normal operations. And such relevant studies are still lacking.

In this paper, a systematic methodology has been developed to examine ozone impacts due to the excess VOCs and NO_x released from regional OGCPI plants when their DRE values are lower than the presumed national standard caused by adverse meteorological and operating conditions. The formulas considering meteorological and operating conditions were derived from CFD and WERF modeling and employed to predict their effects on flare DREs and thus subsequent ozone formations. This study could enrich fundamental understandings of industrial point source emissions and provide the quantitative and valuable support for the ozone pollution caused by OGCPI flare emissions under low DRE instead of standard values.

2. Problem Statement

This paper derives the DRE formula for flare combustion associated with cross-wind speed, flare jet velocity, HVCZ as well as flare design parameters, which are based on both CFD modeling (Jatale et al., 2012; Ge et al., 2018c; Chen and Alphones, 2019) and the studies of WERF (Willi et al., 2013). Next, the elevated point sources from OGCPI emission inventory files (i.e., flare emissions in this study) are extracted and modified based on the derived DRE formula instead of the standard value regulated by Texas Commission on Environmental Quality (TCEQ). DRE values for each flare emissions are calculated and adjusted based on cross-wind speed and jet velocity provided by emission inventory of the studied ozone episode. After that, the number of VOCs and

NO_x from point sources can be obtained due to the incomplete combustion of flare emissions from OGCPI plants. Finally, the emission inventory will be updated and generated by new point source emissions calculated by adjusted DRE values, which will be then employed for the air quality modeling to simulate ozone concentration impacted by the derived DREs. For clarity, the assumptions, given information, and information to be determined for this study are summarized below:

<u>Assumptions:</u>

(1) The studied flare emissions from OGCPI plants will occur in the selected ozone episode in Southeast of Texas, USA;

(2) Compared with the base case air-quality simulation, case studies on ozone impacts will have all of the same modeling inputs as the base case, except the addition of flaring emissions generated due to lower DREs from OGCPI plants in the studied ozone domain.

<u>Given information:</u>

(1) Spatial locations of all flare point source for OGCPI plants in the studied domain;

(2) Jet velocity of each flare point source of the studied OGCPI plants;

(3) Dynamic cross-wind speed at each flaring point source of the studied OGCPI plants;

(4) Geological domain information on the employed episode region;

(5) The (Houston-Galveston-Brazoria) HGB ozone episode during May 31st and June 16th, 2006, which is served as the base case for air-quality modeling and simulation.

<u>Information to be determined:</u>

(1) Flare DRE corrections established based on both CFD and WERF modeling;

(2) Dynamic ozone concentration distribution in the studied region (Southeast Texas) due to the modified flare DREs of the studied OGCPI plants;

3. Methodology

3.1 Methodology framework

The general methodology framework for this study has been summarized and showed in Figure 1. Firstly, both CFD simulations and WERF modeling are employed to obtain DRE profiles, which will be the function of the cross-wind speed, flare jet velocity, HVCZ, flare design and others. Note that the DREs for different elevated point sources are not the same due to the different cross-wind speed and jet velocity at each location of elevated point source. After that, flare emissions (i.e. VOCs and NO_x) are recompiled by the updated DREs for each elevated point source from the ozone episode. Finally, the new emission inventory can be generated and then employed for the air-quality modeling and simulation to investigate the ozone impacts. Note that two Scenarios are performed to investigate the ozone impacts due to the adjusted DRE through CFD and WERF modeling. In this paper, comprehensive air quality model with extensions (CAMx), which is a multi-scale 3-D photochemical modeling system, is employed to simulate the spatial and temporal distribution of ozone concentrations (CAMx User's Guide, 2014). Detailed ozone episodes including emission inventories and meteorological data used as the base for the air-quality modeling is downloaded from the website of TCEQ. The model has been certified by TCEQ as satisfying the modeling guidelines established by U.S. EPA (TexAQS II Field Study, 2016).

Figure 1. General methodology framework.

3.2 Model descriptions

The comprehensive air quality model with extensions (CAMx) is employed in this study to simulate the spatial and temporal distribution of ozone concentration. CAMx is an Eulerian photochemical dispersion model that allows for integrated "one-atmosphere" assessments of tropospheric air pollutants (i.e. ozone, particulates, air toxics, and mercury) over spatial scales ranging from neighborhoods to continents (CAMx, 2014). CAMx has been approved by U.S. EPA as the tool to demonstrate attainment of the federal standards for ozone by some states like Texas.

In this study, CAMx version 4.53 with the CB05 photochemical mechanism was used to obtain ozone concentration distribution. An ozone episode (May 31st, 2006 through June 16th, 2006) provided by TCEQ is selected as the base case model simulation. The selection was mainly based on three reasons: (1) the complete model input data including geological, meteorological as well as emission inventories; (2) the model has been validated to represent the field measured ozone concentrations; and (3) this ozone episode (17 model days) has more serious ozone problems than other episodes. Thus, it would be significant to perform our case studies by selecting this episode. Note that all CAMx simulations were run on a Dell computer with four 3.6 GHz CPUs and 8 GB memories. The employed CAMx model is a nested regional-to-urban scale with grid resolutions of 36×36 km, 12×12 km, 4×4 km, and 2×2 km as shown in Figure 2. In this study, the 2×2 km domain is selected because this domain has the highest resolution; meanwhile, lots of OGCPI plants are located in this domain area.

Figure 2. Illustration of CAMx simulation domains.

3.3 Ozone calculation

The elevated point sources (i.e., industrial flare emissions from OGCPI plants) were modified based on adjusted DRE values. For each flare source, the adjusted DREs is calculated based on CFD or WERF modeling. After that, emissions of VOCs and NO_x are adjusted. New elevated point emission files for CAMx are then established after all flare emissions have been adjusted and recompiled. Note that CAMx simulations provide hourly ozone concentration at each spatial domain grid, which can be represented by the following equation.

$$C_n^{O_3}\left(d,\ h,\mathbf{x}\right)=\mathrm{CAMx}_n\left(d,\ h,\ \mathbf{x},\eta,\mathrm{EIs}\right) \qquad (1)$$

where $C_n^{O_3}\left(d,h,\mathbf{x}\right)$ represents the hourly (the h^{th} hour on d^{th} day during this eposide) ozone concentration of the n^{th} simulation case in the domain grid **x**. CAMx_n represents the *n*-th CAMx simulation case, which needs the adjusted DRE value (i.e., η) for all of flare emissions from OGCPI plants in the studied air-quality domain. EIs represent the emission inventories of the studied ozone episode including elevated point, area, mobile, on-road, biogenic and other emissions.

$C_0^{O_3}\left(d,h,\mathbf{x}\right)$ represents the background ozone concentration of the base case at hour h on day d in grid **x** with the original emission inventories**.** Note that $C_0^{O_3}\left(d,h,\mathbf{x}\right)$ values are obtained by base case simulation and based on the standard DRE value of 98 % for the elevated point emissions. $C_n^{O_3}\left(d,h,\mathbf{x}\right)$ represents the hourly ozone concentration of the n^{th} simulation case at hour h on day d in grid **x.** To quantitatively study the ozone concentration impacted from the adjusted DREs, the amount of ozone difference between adjusted DRE cases and the base case is defined by the following equation.

$$\Delta C_n^{O_3}\left(d,h,\mathbf{x}\right)=C_n^{O_3}\left(d,h,\mathbf{x}\right)-C_0^{O_3}\left(d,h,\mathbf{x}\right),\quad h=0,1,\ldots,23 \qquad (2)$$

where $\Delta C_n^{O_3}(d,h,\mathbf{x})$ represents the hourly ozone difference due to the adjusted DREs at hour h on day d in grid $\mathbf{x}$, ppb. Based on the results of $\Delta C_n^{O_3}(d,h,\mathbf{x})$, the significance of ozone impact from adjusted flare DRE values can be obtained, which could further provide a quantitative technical support to relevant decision makers.

4. Case Studies

4.1 *DRE results obtained through CFD modeling*

CFD simulation shows that four variables affect the DRE of industrial flares: cross-wind speed, jet velocity of flare vent gas, HVCZ, and stoichiometric ratio. Note that the cross-wind speed and jet velocity are available in the air-quality model of the studied ozone episode. The cross-wind speed of each flare emissions can be obtained from the meteorological information, and the jet velocity can be obtained from the emission inventory. Thus, the actual DRE value for each elevated point source (i.e., flare emissions) can be calculated instead of using the assumption of standard DRE value, which could usually underestimate the real amount of flare emissions. For HVCZ and stoichiometric ratio, default values used by CFD simulations were adopted in this study. The default value for HVCZ is 1461.8 btu/scf, and the default value for stoichiometric ratio is 0.3. Based on CFD simulation results from Singh et al. (2014) with approximations, DREs under the specified U and V were obtained by Ge et al., 2018c.

For point source whose cross-wind speed and jet velocity are not specified in CFD modeling, the bilinear interpolation method is adopted to calculate their DREs. For a given interval of the cross-wind speed as [U_1, U_2], and a given interval of jet velocity as [V_1, V_2], the DRE interpolation is specified as follows:

$$\eta_{CFD} = \frac{1}{(U_2 - U_1)(V_2 - V_1)}[\eta_{11}(U_2 - U)(V_2 - V) + \eta_{21}(U - U_1)(V_2 - V) + \eta_{12}(U_2 - U)(V - V_1) + \eta_{22}(U - U_1)(V - V_1)] \quad (3)$$

Based on the bilinear interpolation, the complete relation of η_{CFD} with respect to U and V can be obtained as shown in Figure 3, which is the contour plot of DREs with changes of cross-wind speed and jet velocity. It can be seen that the DREs keep the default value of 98 % when jet velocity is less than 15 m/s. When the jet velocity is larger than 30 m/s and the cross-wind speed is larger than 5 m/s, DREs will be dropped lower than 80 %. Figure 4 shows the minimum and average DREs of flares through CFD modeling. The maximum DREs are always the same as standard value (i.e., 98 %). The minimum DREs ranges from 87 % to 93 % on different episode days because of different meteorological conditions and flaring jet velocities. The average DREs always keep 97.7 %, which implies that the cross-wind speed and jet velocity would not affect DREs for most of flares.

Figure 3. Contour plot of DREs through CFD modeling.

Figure 4. Minimum and average DREs of flares on each Episode day through CFD modeling.

4.2 DRE results obtained through WERF modeling

An alternate flare DRE formula for flares can be obtained and derived from the available literature established by Water Environment Research Foundation (WERF) based on their experimental observations (Willis et al., 2013). The DRE formula based on WERF modeling are shown as bellows:

$$\eta_{\mathrm{WERF}} = 1 - 0.00166\, e^{0.387A}\, \frac{\mathrm{LHV}_{CH_4}}{\mathrm{LHV}_{Flare}} \quad (4)$$

$$A = U / (V\ g\ \phi)^{1/3} \quad (5)$$

where η_{WERF} represents the flare DREs through WERF modeling, LHV_{CH_4} and LHV_{Flare} represent the low heating values of methane and flare, respectively. *A* represents the coefficient of WERF modeling for the DRE calculation. *U* and *V* are still the cross-wind speed and the jet velocity of a flare source, respectively. *g* represents the gravitational acceleration. ϕ represents the flare tip diameter.

The DREs calculated by the equations under different cross-wind speed and jet velocity are tabulated in Table 1. It is worth pointing out that the results shown in Table 1 indicate that the effect of cross-wind speed on DREs only occurs when the jet velocity is less than 10 m/s. When the jet velocity is 1 m/s, the DREs could be as low as 70 % when the cross-wind speed reaches 15 m/s. When the jet velocity is 10 m/s, the DREs would only be dropped to 97 % with the cross-wind speed as high as 15 m/s. When the jet velocity is higher than 10 m/s, the cross-wind speed has no effect on the DREs as indicated in the Table 1.

Table 1. DREs Obtained by the WERF modeling

Figure 6 shows the minimum and average flare DREs during episode simulation based on the WERF correlation equations. It should be pointed out that, although not shown, the maximum DREs are always considered to be 98 %. As indicated in this figure, the minimum DREs (shown in red curve) can be as low as 90 % on the majority of Episode days as shown in Figure 6. The minimum DREs value ranges from 80.2 % to 90.5 % and the average is 85.4 %. However, the average DREs (shown in blue curve) ranges from 93.7 % to 97.4 % and the average is 95.9 %. The DRE difference shown in Figures 4 and 5 indicate that flare DREs value through WERF modeling are greater than the DREs value through CFD modeling, which means more gaseous pollutants are generated based on the calculation through WERF correction equations than CFD modeling.

Figure 5. Minimum and average DREs of flares on each Episode day through WERF modeling.

For each elevated point sources (i.e., flare emissions) of the studied ozone episode, the adjusted DREs are calculated based on Equations (3) and (4) and employed to generate the adjusted emissions of VOCs, NO_x and CO. The adjusted emissions of VOCs, NO_x and CO can be determined by the Equations (6) through (8). So, elevated point sources were modified and updated in the new emission inventory of the studied ozone episode for further air-quality modeling and simulations based on the adjusted DREs. Note that there are total 450 elevated point sources in the studied emission inventory.

$$f_{VOCs} = f_{0,VOCs} \frac{1-\eta}{1-\eta_0} \quad (6)$$

$$f_{NO_x} = f_{0,NO_x} \, \eta / \eta_0 \quad (7)$$

$$f_{CO} = f_{0,CO} \, \eta / \eta_0 \quad (8)$$

where $f_{0,VOCs}$, f_{0,NO_x} and $f_{0,CO}$ are the amount of original emissions of VOCs, NO_x and CO based on the standard DRE (η_0, i.e., 98 %) for flare combustion. η represents the η_{CFD} or η_{WERF}. f_{VOCs}, f_{NO_x} and f_{CO} are the amount of the updated emissions based on the adjusted DREs through the CFD or WERF modeling.

4.3 Air-quality simulation results based on CAMx modeling

The modified emission inventory files are input into CAMx model for air quality simulations. As mentioned in Section 3.2, an ozone episode established by TCEQ was served as the base case for air quality modeling and simulation. Firstly, the modeling was run once as the base case to get the background ozone concentrations with the original emission inventories. Secondly, the air quality modeling was run again to get ozone concentrations with the updated emission inventories, which are modified by the new elevated point sources changed with the adjusted DREs through CFD or WERF modeling. After that, results from two runs were compared to quantify the effect of the lower flare DREs on regional ozone pollution. CAMx model contains 28 layers started from the earth surface to 14,664 m height. Also, the simulation results of each layer contain 1,575,936 (4104 × 24 × 16) ozone data due to 4,104 (74 × 56) grid cells, 24 hours a day and total 16 simulated days in the studied ozone episode. However, only ground-level ozone is designated as the ozone NAAQs according to EPA's regulation. So, to be simplified in this study, the maximum and minimum ground-level (i.e., first layer, 34 m thickness) ozone difference of each Episode day were selected to investigate the ozone impact due to the adjusted DREs for flares of OGCPI plants.

Figure 6 shows maximum ozone increment and decrement on each Episode day in the 2 × 2 km domain for Scenario I. It can be seen that the maximum hourly ozone increment ranges from 0.002 to 0.18 ppb. The maximum hourly ozone decrement ranges from 0 to 0.03 ppb. Note that the individual DREs could be significantly changed by the atmospheric cross-wind speed and flare jet velocity (e.g., the adjusted DREs can be as low as 74 % at a jet velocity of 40 m/s and a cross-wind speed of 15 m/s.). However, case studies show that the regional ozone impact will not be affected much because the maximum hourly ozone increment is only 0.18 ppb. HVCZ and stoichiometric ratio for flare combustion are fixed as normal values in CFD modeling. Thus, these two impact factors on DREs value are neglected. Figure 7 shows maximum ozone increment and decrement on each Episode day in the 2 × 2 km domain for Scenario II. It can be seen that the maximum hourly ozone increment can range from 0.001 to 1.3 ppb. The maximum hourly ozone decrement can range from 0 to 0.3 ppb. Figure 8 shows the ozone spatial distribution on the day of the maximum ozone increment for two Scenarios. The maximum ozone increment for Scenarios I and II happened at 6:00 am on June 11, 2006 and at 10:00 am on June 13, 2006, respectively. The corresponding locations of the maximum ozone increment for two Scenarios are shown in Figure 8.

Figure 6. Maximum ozone increment and decrement on each Episode day in Scenario I.

Figure 7. Maximum ozone increment and decrement on each Episode day in Scenario II.

Figure 8. Ozone spatial distribution on the day of the maximum ozone increment for two Scenarios.

5. Conclusions

By coupling dynamic flaring DREs of OGCPI plants with CAMx based air-quality modeling and simulation, the ground-level ozone impact associated with meteorological and process operating conditions have been quantitatively studied in this work. The CFD and WERF modeling based DRE correlations have been investigated respectively. Through case studies, it shows that although the individual DREs through CFD modeling could be significantly changed by the atmospheric cross-wind speed and flare jet velocity, the regional ozone impacts will not be affected too much (only 0.18 ppb). However, the maximum hourly ozone increment is 1.3 ppb through WERF modeling by considering the HVCZ and flare design. Note that this is the initial study coupling process DRE estimation and regional air-quality impacts to evaluate the ozone pollution situation under the estimated DREs instead of standard value. This study could enrich fundamental understandings of industrial point source emissions and provide the quantitative and valuable support for the ozone pollution caused by OGCPI flare emissions under low DRE instead of standard values.

Acknowledgement

This work was supported in part by Texas Air Research Center (TARC), as well as Graduate Student Scholarship and Anita Riddle Faculty Fellowship from Lamar University in USA.

Nomenclature

Abbreviations:

CAMx	Comprehensive Air Quality Model with Extensions
CFD	Computational Fluid Dynamics
DRE	Destruction and Removal Efficiency
EPA	Environmental Protection Agency of USA
HGB	Houston-Galveston-Brazoria
HRVOCs	Highly Reactive Volatile Organic Compounds
HVCZ	Heating Value of Combustion Zone
LHV	Low Heating Value
NAAQs	National Ambient Air Quality Standards
NO_x	NO/NO_2
OGCPI	Oil, Gas & Chemical Process Industries
TCEQ	Texas Commission on Environmental Quality
VOCs	Volatile Organic Compounds
WERF	Water Environment Research Foundation

Indexes:

A	Index of the coefficient of WERF modeling for DRE calculation
d	Each day during the selected episode
EIs	Index of emission inventories
g	Index of the gravitational acceleration

h Index of the time of day

n Index of n[th] CAMx simulation case

$\mathbf{x}$ Index of a domain grid

Parameters and variables:

U Atmospheric cross-wind speed

V Flare jet velocity

CAMx_n The *n*-th CAMx simulation case

$C_0^{O_3}(d,h,\mathbf{x})$ Background ozone concentration of the base case at hour h on day d in grid $\mathbf{x}$

$C_n^{O_3}(d,h,\mathbf{x})$ The hourly ozone concentration of the n^{th} simulation case at hour h on day d in grid $\mathbf{x}$

$\Delta C_n^{O_3}(d,h,\mathbf{x})$ The hourly ozone difference due to the adjusted $\eta(U,V)$ at hour h on day d in grid $\mathbf{x}$

$f_{0,VOC}$ The amount of VOCs emissions from the elevated point sources in the studied ozone episode

f_{0,NO_x} The amount of NO_x emissions from the elevated point sources in the studied ozone episode

$f_{0,CO}$ The amount of CO emissions from the elevated point sources in the studied ozone episode

f_{VOC} The adjusted VOCs emissions based on the adjusted DRE formula

f_{NO_x} The adjusted NO_x emissions based on the adjusted DRE formula

f_{CO} The adjusted CO emissions based on the adjusted DRE formula

η The adjusted DRE value for flare combustion

η_0 Standard DRE value

ϕ Flare tip diameter

References

Aalsalem, M.Y., Khan, W. Z., Gharibi, W., Khan, M. K., and Arshad, Q. Wireless Sensor Networks in oil and gas industry: Recent advances, taxonomy, requirements, and open challenges. Journal of Network and Computer Applications. 2018, 113, 87-97.

Allen D.T. Combining innovative science and policy to improve air quality in cities with refining and chemicals manufacturing: The case study of Houston, Texas, USA. Frontiers of Chemical Science and Engineering. 2017, 11(3): 293-304.

American Petroleum Institute (2008). ANSI/API Standard 537. Flare Details for General Refinery and Petrochemical Service. Washington, DC, USA.

Baukal CE, Schwartz RE. (2001). The John Zink Combustion Handbook. New York, CRC Press.

CAMx User's Guide: Comprehensive Air Quality Model with Extensions version 4.53. Novato, California, April, 2014.

Castiñeira, D., Edgar, T.F. CFD for simulation of crosswind on the efficiency of high momentum jet turbulent combustion flames. Journal of Environmental Engineering. 2008, 134(7): 561-571.

Chen, D.H., Alphones, A. Characterization of the incipient smoke point for steam-/air-assisted and nonassisted flares. Journal of the Air & Waste Management Association. 2019, 69(1): 119-130.

Cleveland, W. S; Graedel, T. E, Kleiner, B; Warner, K.L. Sunday and workday variations in photochemical air pollutants in New Jersey and New York. Science. 1974;186(4168):1037-1038.

Kampa, M; Castanas, E. Human health effects of air pollution. Environmental pollution. 2008,151(2):362-367.

EPA. National Ambient Air Quality Standards. Available online at https://www. epa.gov/criteria-air-pollutants/naaqs-table. Accessed March 29, 2016.

Ge, S.J., Wang, S.J., Xu, Q., Ho, T. Air-quality considered study for multiple olefin plant startups. *Industrial & Engineering Chemistry Research*. 2016. 55(36):9698-9710.

Ge, S.J.; Wang, S.J.; Xu, Q.; Ho, T.C. Impact of chemical plant start-up emissions on ambient ozone concentration. *Atmospheric Environment*. 2017, 164, 20-30.

Ge, S.J.; Wang, S.J.; Xu, Q.; Ho, T.C. Ozone impact minimization through coordinated scheduling of turnaround operations from multiple olefin plants in an ozone nonattainment area. *Atmospheric Environment*. 2018a, 176: 47-53.

Ge, S.J.; Wang, S.J.; Xu, Q.; Ho, T. Study on regional air quality impact from a chemical plant emergency shutdown. *Chemosphere*. 2018b, 201: 655-666.

Ge, S., Wang, S., Zhang, J., Xu, Q.; Ho, T. (2018). Modelling and Simulation for Regional Ozone Impact by Flaring Destruction and Removal Efficiency of Oil & Gas Industries. *Computer Aided Chemical Engineering*. 2018c, 44: 2185-2190.

Ge, S.J.; Zhang, J.; Wang, S.J.; Xu, Q.; Ho, T. New insight of ozone pollution impact from flare emissions of chemical plant start-up operations. *Environmental Pollution*. 2019, 245:873-882.

Jatale, A.; Smith, P.; Thornock J.; and Smith, S. A validation of flare combustion efficiency simulations. American Flame Research Committee, Salt Lake City, UT. 2012.

McDaniel, M. Flare Efficiency Study; United States Environmental Protection Agency: Washington, DC, Report No. 600/2-83-052, July 1983.

Pohl, J. H. Evaluation of the Efficiency of Industrial Flares; United States Environmental Protection Agency: Washington, DC, Report Nos. EPA600-2-85-95 and EPA600-2-85-106, 1984/1985.

Singh, K.D., Dabade, T., Vaid, H., Gangadharan, P., Chen, D., Lou, H.H., Li, X., Li, K. and Martin, C.B. Computational Fluid Dynamics Modeling of Industrial Flares Operated in Stand-By Mode. Industrial & Engineering Chemistry Research. 2012, 51(39): 12611-12620.

Singh, K.D., Gangadharan, P., Dabade, T., Shinde, V., Chen, D., Lou, H.H., Richmond, P.C. and Li, X. Parametric Study of Ethylene Flare Operations Using Numerical Simulation. Engineering Applications of Computational Fluid Mechanics. 2014, 8(2): 211-228.

Texas Commission on Environmental Quality (TCEQ). 2013 Emission Inventory Guidelines, Appendix A: Technical Supplements. Available online at http://www.tceq.state.tx.us/publications/rg/rg-360-13/index.html. Accessed June 5, 2015.

TexAQS II Field Study. Available online at: https://www.tceq.texas.gov/airquality/research/texaqs. Accessed December 5, 2016.

Xu, Q; Li, K.Y. Dynamic Simulation for Chemical Plant Turnaround Operation. Integrated Environmental Management Consortium Meeting, Houston, Texas, June 25, 2008.

Xu, Q.; Yang, X.T.; Liu, C.W.; Li, K; Lou., H.H; Gossage., J.L. Chemical plant flare minimization via plant-wide dynamic simulation. Industrial & Engineering Chemistry Research. 2009, 48(7): 3505-3512.

Willis J.; Checkel D.; Handford D.; Shah A.; Joiner M. Final Report: Flare Efficiency Estimator and Case Studies. Water Environment Research Foundation, 2013.

List of Table

Table 1. DREs Obtained by the WERF modeling

U \ V_j	**1**	**3**	**5**	**10**	**15**	**20**	**25**	**30**	**35**	**40**
0.1	98%	98%	98%	98%	98%	98%	98%	98%	98%	98%
1	98%	98%	98%	98%	98%	98%	98%	98%	98%	98%
3	98%	98%	98%	98%	98%	98%	98%	98%	98%	98%
5	98%	98%	98%	98%	98%	98%	98%	98%	98%	98%
7	97%	98%	98%	98%	98%	98%	98%	98%	98%	98%
9	94%	98%	98%	98%	98%	98%	98%	98%	98%	98%
11	87%	96%	98%	98%	98%	98%	98%	98%	98%	98%
13	72%	94%	96%	98%	98%	98%	98%	98%	98%	98%
15	70%	89%	94%	97%	98%	98%	98%	98%	98%	98%

Note: the unit of crosswind speed (U) and the jet velocity (V) are both m/s.

List of Figures

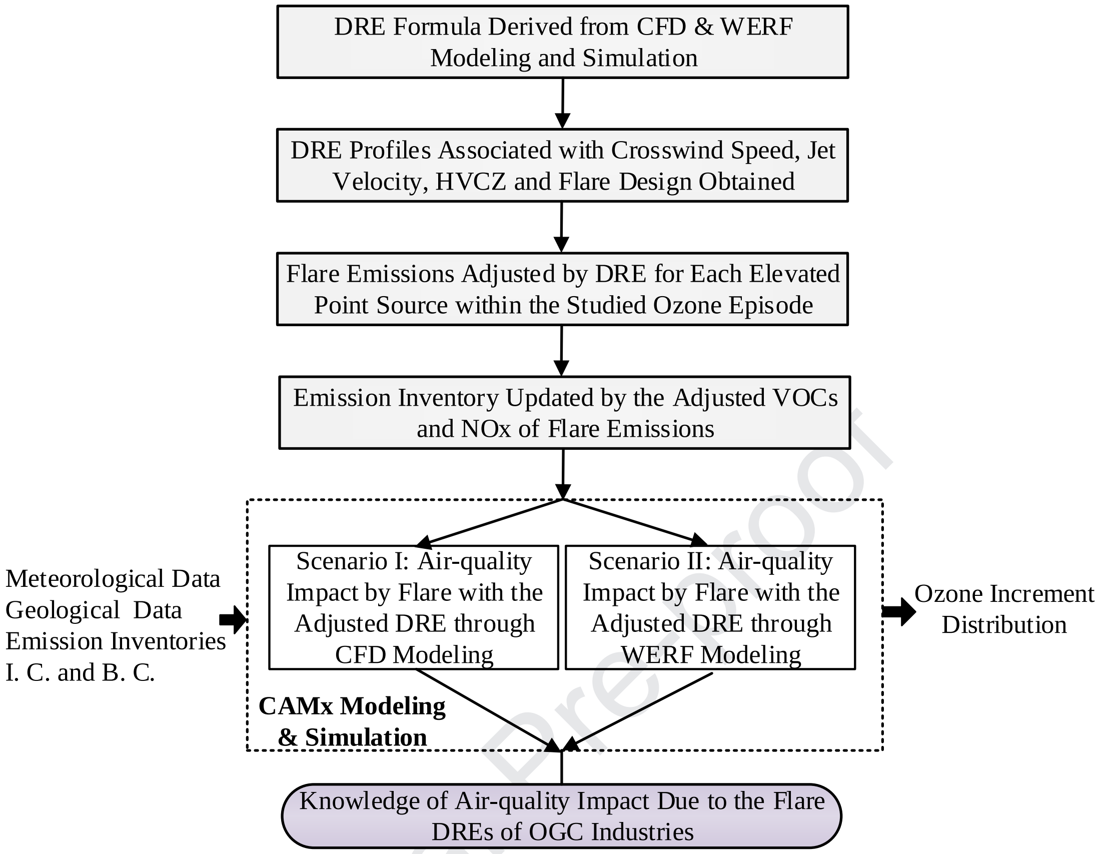

Figure 1. General methodology framework.

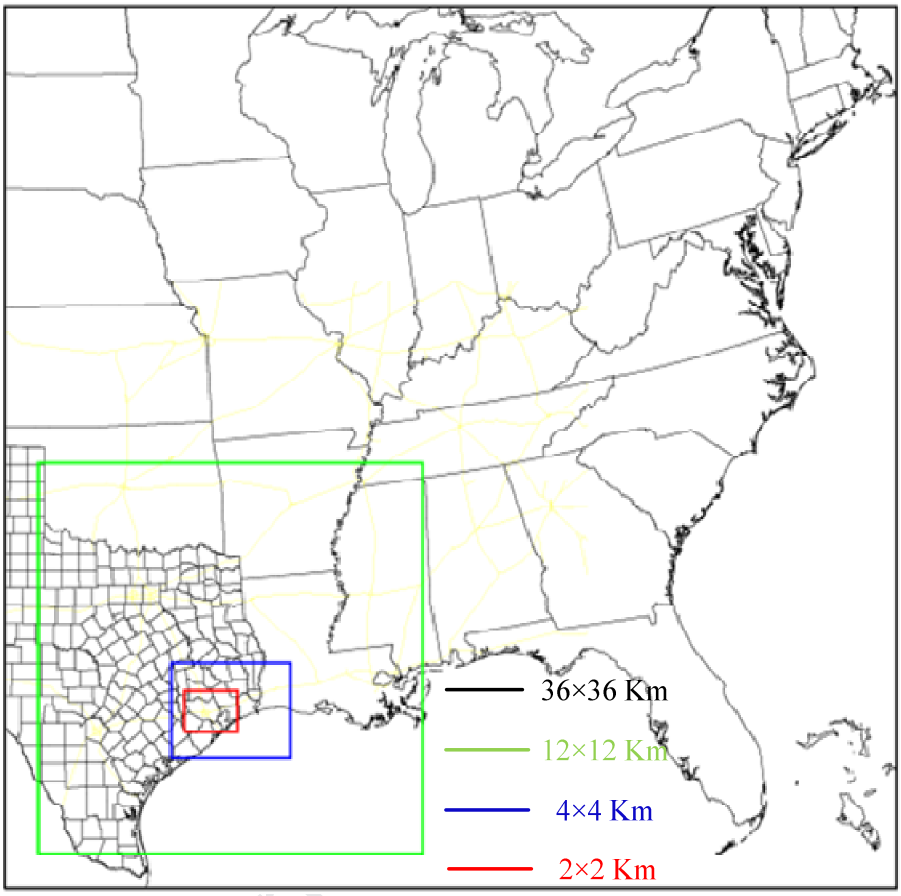

Figure 2. Illustration of CAMx simulation domains.

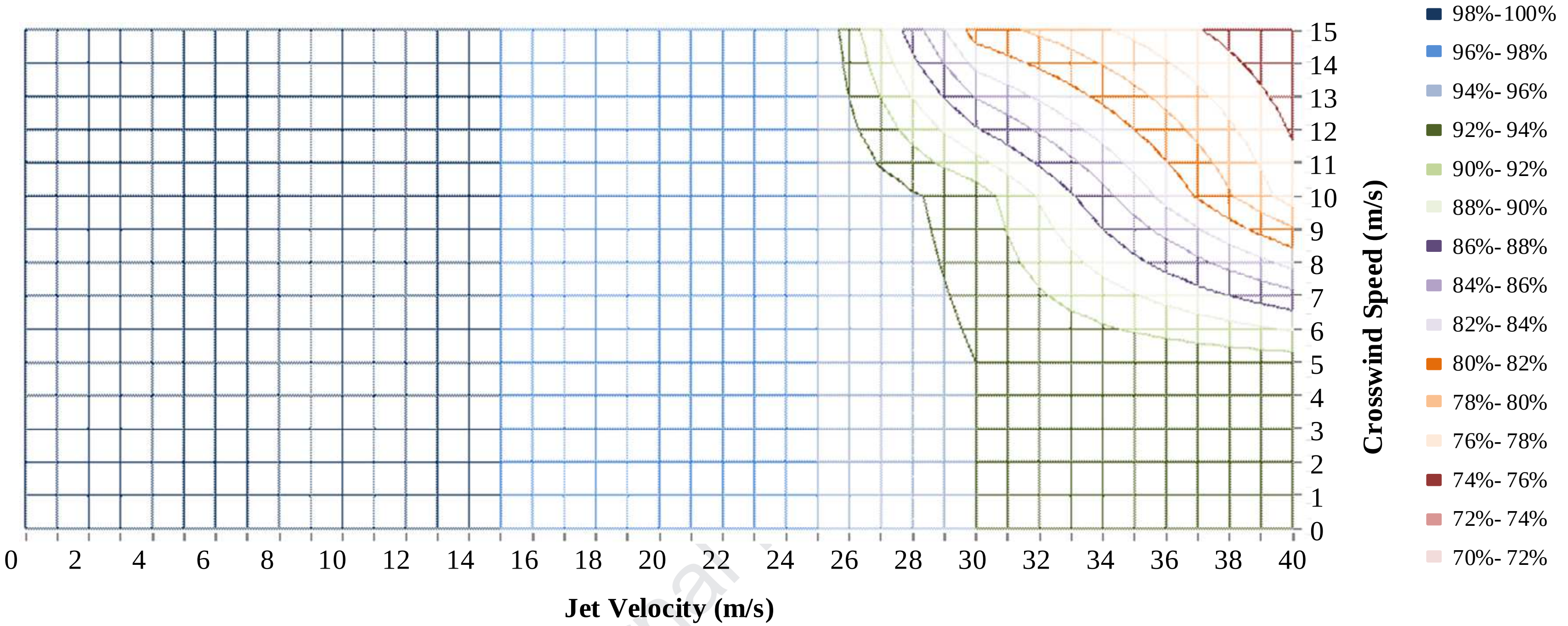

Figure 3. Contour plot of DREs through CFD modeling.

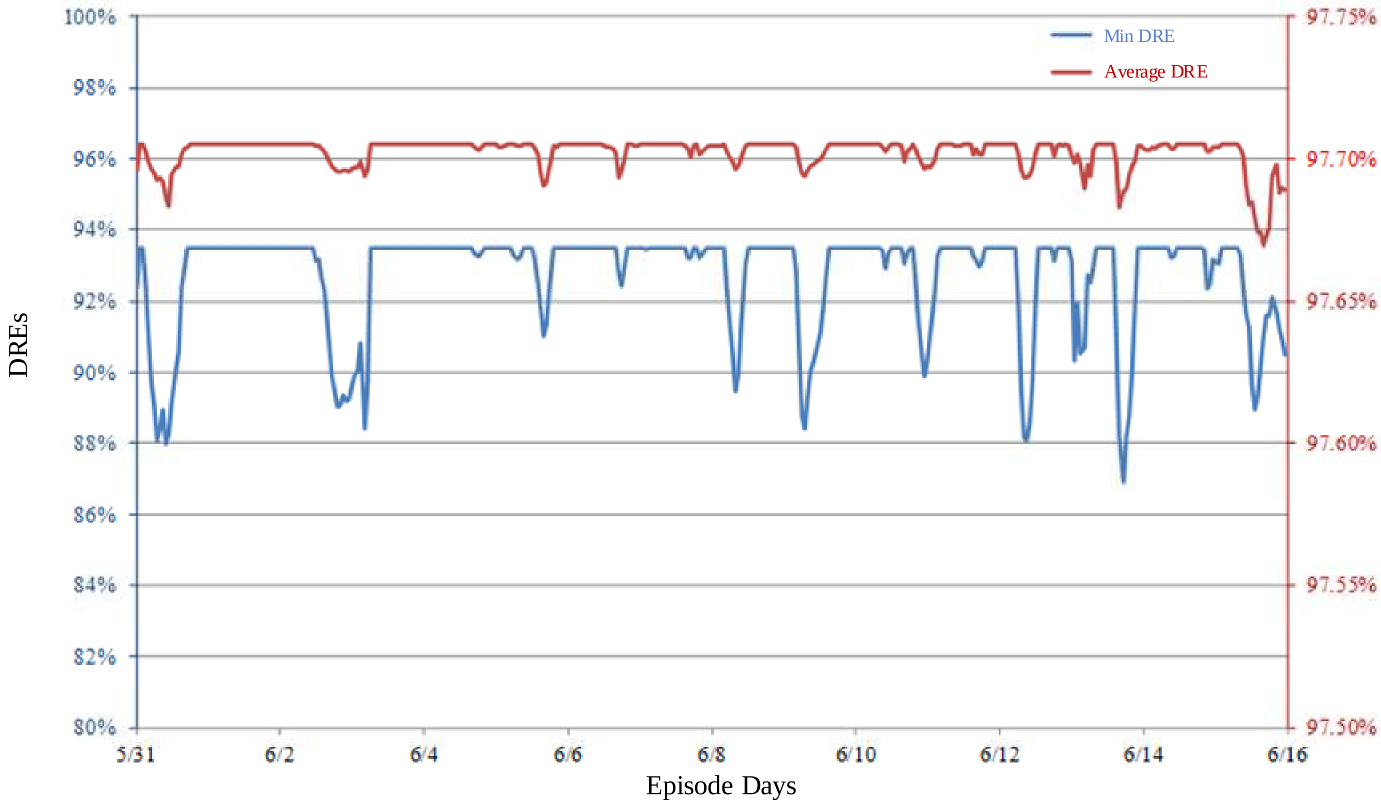

Figure 4. Minimum and average DREs of flares on each Episode day through CFD modeling.

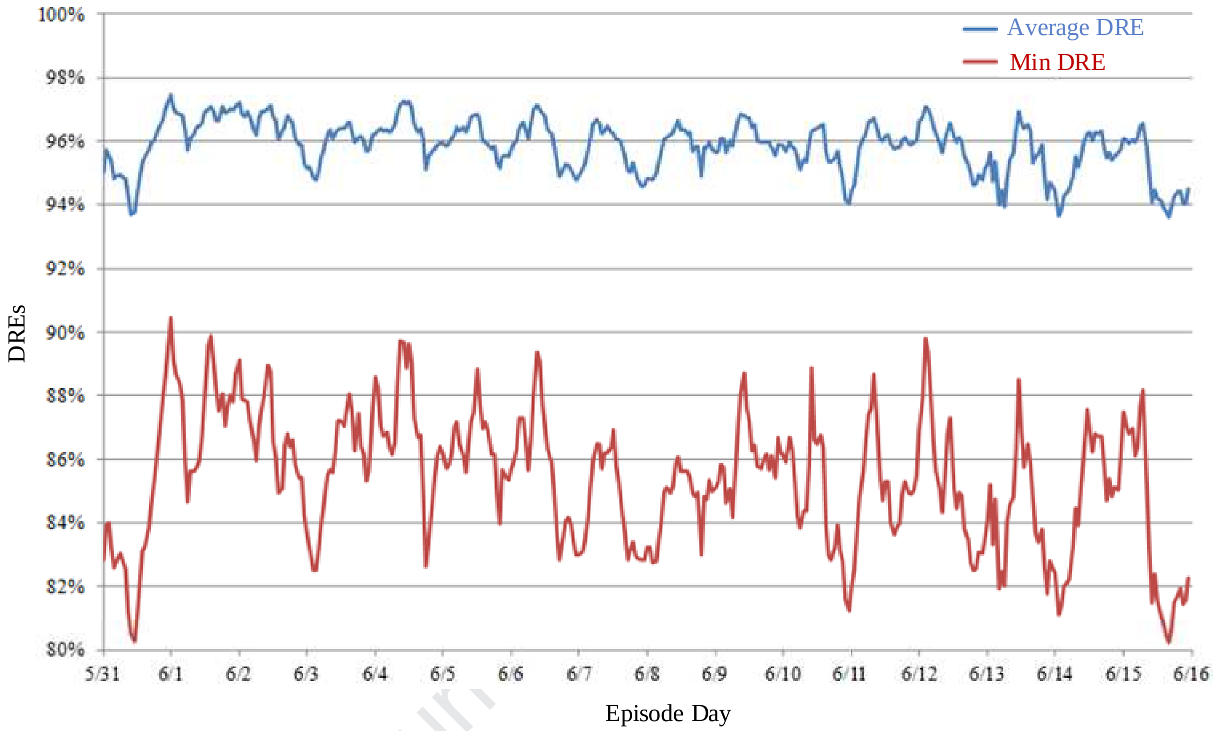

Figure 5. Minimum and average DREs of flares on each Episode day through WERF modeling.

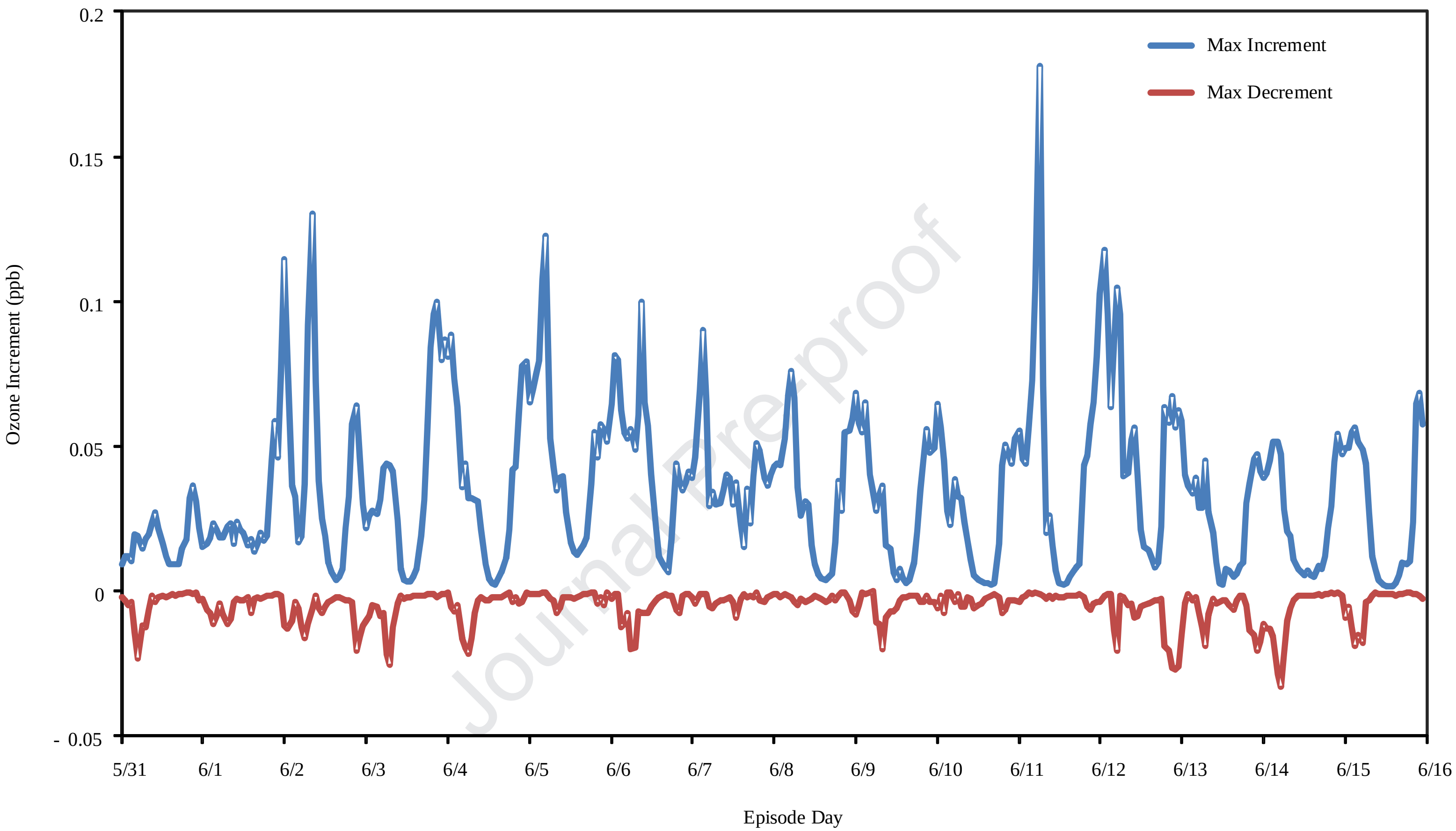

Figure 6. Maximum ozone increment and decrement on each Episode day in Scenario I.

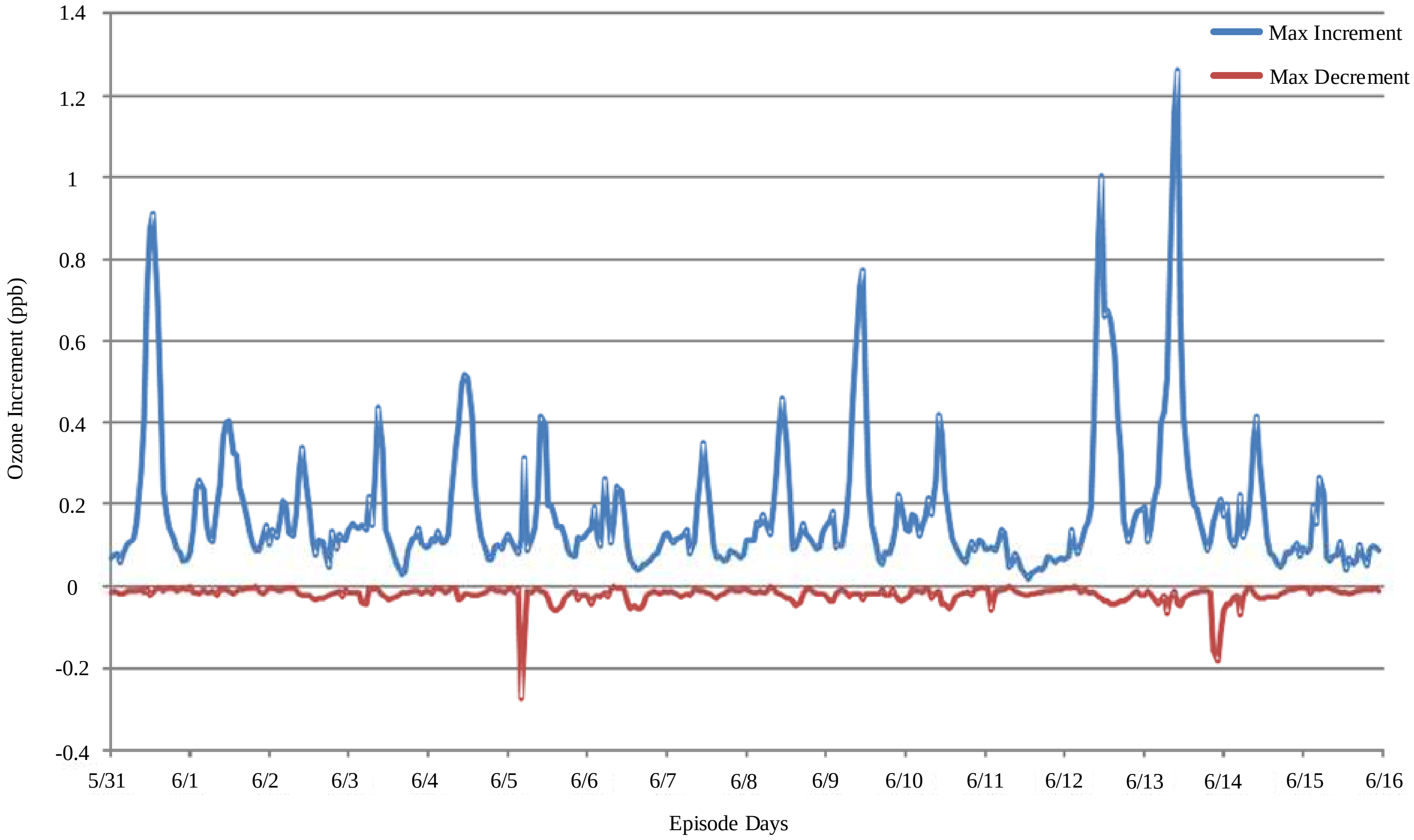

Figure 7. Maximum ozone increment and decrement on each Episode day in Scenario II.

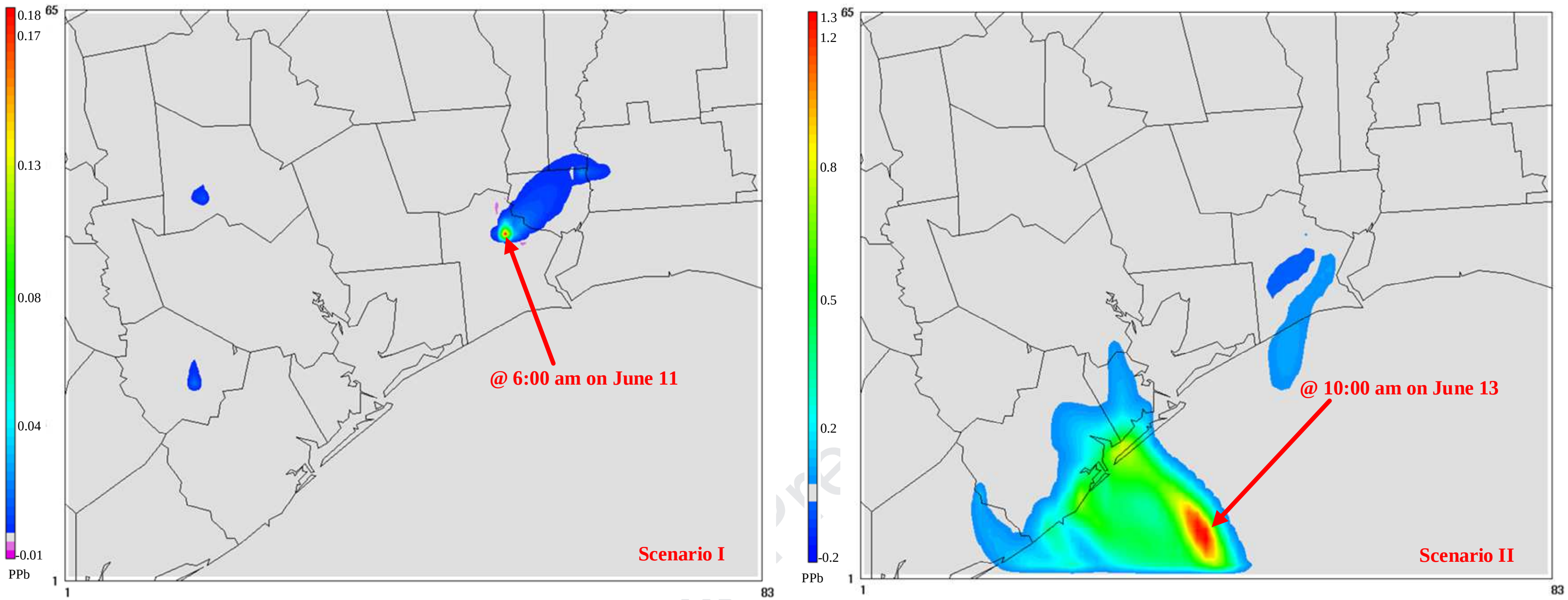

Figure 8. Ozone spatial distribution on the day of the maximum ozone increment for two Scenarios.

Highlights

- Coupling Dynamic Flaring DREs with CAMx Modeling for Ozone Simulation
- Flare DRE corrections established based on both CFD and WERF modeling
- Effect of Flare DRE on Regional Ozone Pollution from OGCPI

Declaration of Interest Statement

The authors declare that they have no known competing financial interests or personal relationships that could have appeared to influence the work reported in this paper.